Electron collisions with F_2CO molecules

Thiago Corrêa Freitas*
Tecnologia em Luteria, Universidade Federal do Paraná, 81520-260 Curitiba, Paraná, Brazil

Alessandra Souza Barbosa and Márcio Henrique Franco Bettega
Departamento de Física, Universidade Federal do Paraná, Caixa Postal 19044, 81531-990 Curitiba, Paraná, Brazil

(Received 17 April 2017; published 11 July 2017)

In this paper we present elastic differential, integral, and momentum-transfer cross sections for electron collisions with carbonyl fluoride (F_2CO) molecules for the incident electron's energy from 0.5 eV to 20 eV. The Schwinger multichannel method with pseudopotentials was employed to obtain the cross sections in the static-exchange and static-exchange plus polarization approximations. The present results were compared with the available data in the literature, in particular, with the results of Kaur, Mason, and Antony [Phys. Rev. A **92**, 052702 (2015)] for the differential, total, and momentum-transfer cross sections. We have found a π^* shape resonance centered at 2.6 eV in the B_1 symmetry and other resonance, in the B_2 symmetry, located at around 9.7 eV. A systematic study of the inclusion of polarization effects was performed in order to have a well balanced description of this negative-ion transient state. The effects of the long-range electric dipole potential were included by the Born closure scheme. Electronic structure calculations were also performed to help in the interpretation of the scattering results, and associate the transient states to the unoccupied orbitals.

DOI: 10.1103/PhysRevA.96.012702

I. INTRODUCTION

Electron collisions with molecules related to the atmospheric pollution, like chlorofluorcarbons (CFCs) or their substitutes, have been the motivation of several papers after the Kyoto protocol [1]. Hydrofluorcarbons (HFC) are used as refrigerants in replacement of CFCs, and the breakdown of one of them (CF_3CH_2F, also known as HCF-134a), after a series of complex reactions in the troposphere, results in F_2CO and HF [2]; the reaction between CF_3O and NO also leads to the F_2CO and FNO [3], suggesting a probable increase in the concentration of carbonyl fluoride in the atmosphere.

Some technological applications of carbonyl fluoride are in the replacement of others cleaners of chemical vapor deposition chambers [4], and the use as a plasma feed gas in solar cell manufacture [5] in a pressure equal or greater than the atmospheric pressure. Early studies on the production of F_2CO, ultraviolet absorption, photoelectron and VUV photoabsorption were carried out in Refs. [6–12] more than four decades ago. The vertical electronic spectrum of this molecule was investigated by Vasudevan and Grein [13]. Sherwood *et al.* [14] performed a photoelectron spectra experiment of F_2CO. A theoretical study about the UV and photoelectronic spectra was carried out by Grein [13]. The Rydberg transitions intensities were computed by Olalla *et al.* [15], and Choi and Baeck [16] performed a series of calculations to study the spectroscopic constants of the ground state and some low-lying excited states. Kato *et al.* [17] performed a high-resolution electron impact vibrational excitation of carbonyl fluoride experiment, together with a comparative study with H_2CO. In a recent paper, Kato *et al.* [18] also obtained the energy loss spectra (EELS) for F_2CO in the range 5 eV to 18 eV.

Hoshino *et al.* [19] have investigated dissociative electron attachment (DEA) to carbonyl fluoride by means of a crossed electron-molecular beam experiment. The incident electron energy range was from 0 eV to 30 eV. Quantum chemical calculations were performed to support the experimental analysis. They have found the following fragment ions formation: F^-, F_2^-, and COF^-, with their respective most intense signals centered at 2.15 eV, 2.40 eV, and 2.62 eV. The group also suggest these anion formations are related to a π^* resonance.

Theoretical calculations of electron scattering by carbonyl fluoride were performed by Kaur *et al.* [20] using the *ab initio* *R*-matrix method from 0.5 eV to 30 eV, and spherical complex optical potential methods from 30 eV to 5000 eV. They have obtained differential, momentum transfer, total, total ionization, and electronic excitation cross sections. In the total cross section (TCS), at low-energy range, a π^* resonance was reported centered at 4.23 eV and 3.67 eV in their static-exchange (SE) and static-exchange plus polarization (SEP) approximations, respectively. The momentum transfer cross section was calculated from 0.5 eV to 20 eV, and differential cross sections (DCS) were presented for selected energies of 1 eV, 3 eV, 6 eV, 9 eV, 12 eV, and 15 eV.

In this paper we present integral, differential, and momentum transfer cross sections for elastic electron collisions with F_2CO in the static-exchange and static-exchange plus polarization approximations, for the energy range 0.5 eV to 20 eV, using the Schwinger multichannel method with pseudopotentials. In Sec. II we will briefly describe the method and the computational details, Sec. III is dedicated to the results and discussions, and the paper ends with a summary of our findings.

II. THEORY AND COMPUTATIONAL DETAIL

The Schwinger multichannel method (SMC) and its implementation with pseudopotentials (SMCPP) have been described in detail elsewhere [21–25]. Here we will only describe the relevant points of the method concerning the present work. The SMC method is a variational approach to the scattering

*tcf@ufpr.br

amplitude that results in the following working expression:

$$f(\mathbf{k_f},\mathbf{k_i}) = -\frac{1}{2\pi}\sum_{m,n}\langle S_{\mathbf{k}_f}|V|\chi_m\rangle(d^{-1})_{mn}\langle\chi_n|V|S_{\mathbf{k}_i}\rangle, \quad (1)$$

where

$$d_{mn} = \langle\chi_m|A^{(+)}|\chi_n\rangle \quad (2)$$

and

$$A^{(+)} = \frac{\hat{H}}{N+1} - \frac{(P\hat{H}+\hat{H}P)}{2} + \frac{(PV+VP)}{2} - VG_P^{(+)}V. \quad (3)$$

In the above equations, $|S_{\mathbf{k}_{i,f}}\rangle$ is a solution of the unperturbed Hamiltonian H_0 and is a product of a target state and a plane wave, V is the interaction potential between the incident electron and the molecular target, $\{|\chi_m\rangle\}$ is a set of $(N+1)$-electron Slater determinants, called configuration state functions (CSFs), used in the expansion of the trial scattering wave function, $\hat{H} = E - H$ is the collision energy minus the full Hamiltonian of the system, with $H = H_0 + V$, P is a projection operator onto the open-channel space defined by the target eigenfunctions, and $G_P^{(+)}$ is the free-particle Green's function projected on the P space.

In the static-exchange (SE) approximation, the $(N+1)$-electron basis is constructed as $|\chi_n\rangle = \mathcal{A}|\Phi_1\rangle \otimes |\varphi_n\rangle$, where $|\Phi_1\rangle$ is the Hartree-Fock target ground state, $|\varphi_n\rangle$ is a single-particle function, and $\mathcal{A}$ is the antisymmetrizer. In the static-exchange plus polatization (SEP) approximation, the SE set is enlarged by including CSFs constructed as $|\chi_{mn}\rangle = \mathcal{A}|\Phi_m\rangle \otimes |\varphi_n\rangle$, where $|\Phi_m\rangle$ are N-electron Slater determinants which are obtained by performing single excitations of the target and $|\varphi_n\rangle$ is also a single-particle function.

Our calculations were carried out at the equilibrium geometry available in the literature [26], in the C_{2v} point group, and the geometrical structure of the molecule is shown in Fig. 1. Pseudopotentials of Bachelet, Hamann, and Schlüter [27] are used to replace, in this case, the atomic $1s$ core electrons of C, O, and F. The single particle $5s$, $5p$, $2d$ basis set used to represent the target ground state and the scattering orbitals were generated following the procedure described in Ref. [28]. The exponents of the Cartesian-Gaussian functions for C and O are the same as used by Kossoski, Bettega, and Varella [29]. For the F atoms, the exponents are as follows: 6.075502, 1.706018, 0.988089, 0.517617, and 0.097670 for the s-type functions; 15.82934, 4.972119, 1.731288, 0.597893, and 0.193221 for p-type functions; d-type functions are from Ref. [30]; for all the functions the contraction coefficients are equal to 1.0. The symmetric combinations of the d-type functions were not included in our calculations to avoid linear dependency in the basis set.

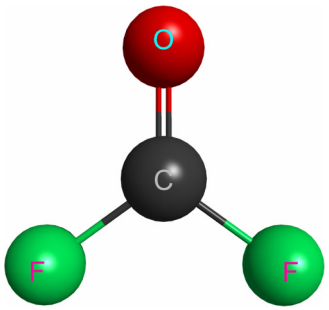

FIG. 1. Geometrical structure of F_2CO molecule generated with MacMolPlt [38].

To take polarization effects into account we employed the modified virtual orbitals (MVOs) [31] generated for a +6 cationic operator to represent the particle and the scattering orbitals. All singlet- and triplet-coupled excitations from the 12 occupied orbitals to the 45 lowest MVOs are considered in the construction of the CSFs for the A_1, B_2, and A_2 symmetries. The same set of MVOs were used as scattering orbitals. We obtained 6361 CSFs for the A_1 symmetry, 6227 CSFs for the B_2 symmetry, and 5845 CSFs for the A_2 symmetry.

In order to understand the role of the polarization effects, several different SEP calculations were performed for the resonant B_1 symmetry. A sequence of calculations using only singlet-coupled excitations always from the 12 occupied orbitals to the 45, 60, 69, 74, and 81 lowest MVOs, with the same MVOs as scattering orbitals, were performed. The number of CSFs obtained for each calculation, labeled as S1 to S5, was 2637, 5287, 6957, 7995, and 9453, respectively. The inclusion of triplet-coupled excitations may lead to an overcorrelation in the polarization description, placing the transient state in a lower-energy position than the experimental data (when available), and since this symmetry is essentially resonant with only a small contribution from background scattering, this is a good way of including polarization effects without introducing overcorrelation [32] in a resonant symmetry. Another possible way to describe the π^* state with well balanced polarization effects is performing singlet-coupled excitations only from the hole orbital and particle orbitals belonging to the same symmetry, and consider only the resonant MVO as scattering orbital [33]. With this procedure, calculation labeled as SEP-SM, all the resonant configurations are active, leading to 519 CSFs.

F_2CO molecule has permanent dipole moment, the present computed value is 1.18 D, the calculated value by Kaur *et al.* [20] is 0.89 D, and the experimental values available in the literature are 1.03 D [19] and 0.95 D [34]. The well-known Born closure [35,36] scheme was employed to take the long-range character of the dipole interaction into account and compute the differential and integral cross sections. In this procedure, the low partial wave contributions are

TABLE I. Values of $\ell_{\max}$ used in the Born closure scheme in the SE and SEP approximations.

$\ell_{\max}$	SE	SEP
1	0.5–1.9 eV	0.5–1.4 eV
2	2–2.4 eV	1.5–2.3 eV
3	2.5–3.8 eV	2.4–5 eV
4	3.9–7 eV	5.5–6.5 eV
5	7.5–8 eV	7 eV
6	8.5–11.5 eV	7.5–8 eV
7	12–14 eV	8.5–9.5 eV
8	14.5–16.5 eV	10–17.5 eV
9	17–20 eV	18–20 eV

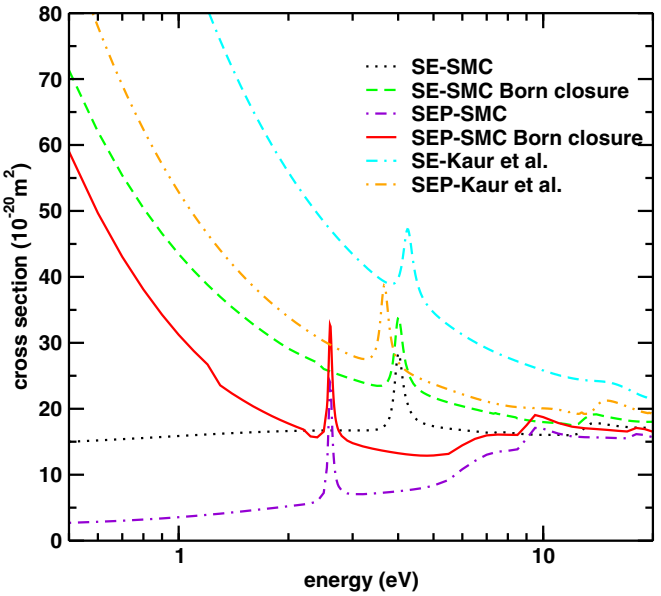

FIG. 2. Integral elastic cross section in the SE (dotted line), SE with Born closure (dashed line), SEP (dot-dashed line), and SEP with Born closure (solid line) approximations. TCS obtained by Kaur *et al.* [20] using the *R*-matrix method, in the SE (dot-dash-dashed line) and SEP (dot-dot-dashed line) approximations with Born correction, is also shown for comparison purposes. See text for discussion.

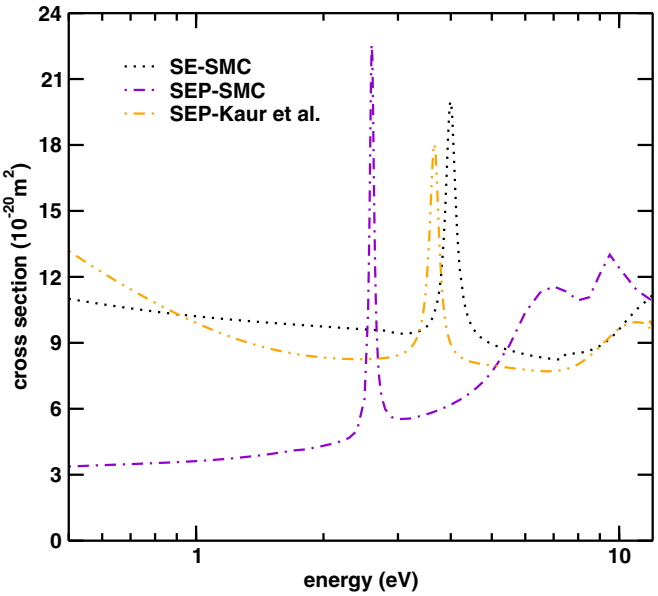

FIG. 3. Momentum-transfer cross section in the SE (dotted line), and SEP (dot-dashed line) approximations. The momentum-transfer cross section obtained by Kaur *et al.* [20], using the *R*-matrix method in SEP approximation (dot-dot-dashed line), is also shown for comparison purposes. See text for discussion.

retained until a certain $\ell_{\max}$ value and the higher partial wave contributions are obtained in the first Born approximation for a point dipole moment with the same magnitude and orientation as the molecular dipole. In order to avoid the divergence of the forward scattering amplitude, we employed an approximation that accounts for the inelastic dipole-allowed rotational transitions (00 $\longrightarrow$ 10 rotational excitation of an asymmetric top) [37], by making $k_f^2 = k_i^2 + 2\Delta E_{\rm rot}$, where $\Delta E_{\rm rot} = 2.37540\times10^{-5}$ eV. For SE and SEP calculations, the values of $\ell_{\max}$ are summarized in Table I.

III. RESULTS AND DISCUSSION

Figure 2 shows the integral elastic cross section obtained in the SE and SEP approximations with and without the Born closure scheme. The SE results show a peak located at around 4 eV and a shoulder located near 14 eV. The inclusion of the long-range dipole scattering with the Born closure procedure affects the magnitude of the cross section mainly below 3 eV. With the inclusion of the polarization effects, SEP results, the structures centered at 4 eV and 14 eV move to around 2.6 eV and 9.5 eV, respectively. A noticeable soft peak appears in the SEP calculations located at 7 eV. The structures we have found at around 2.6 eV, 7 eV, and 9.5 eV are in agreement, as expected, with the experimental results for electron impact vibrational excitation of Kato *et al.* [17], that reported structures at around 2 eV and 7.5–10 eV.

The increase of the cross section in the SEP approximation with Born closure as energy vanishes is more noticeable for energies below 3 eV. The Born closure scheme employed by us usually overestimates the magnitude of the integral cross section for the low-energy range; the same behavior was also pointed out by Kaur *et al.* about their Born correction implementation. The overestimation of approximately 67% at 1 eV for reference of their SEP-TCS over the present SEP+Born closure calculations may be partially due to an artifact of that procedure. The results of Kaur *et al.* [20] in the SE approximation show a structure at around 4.23 eV, and the SEP calculations put this peak centered at 3.67 eV. The difference in energy of the π^* resonance between present SE calculations and the *R*-matrix results by Kaur *et al.* [20] may be mainly due to the different geometries used to perform the calculations. The differences in the SEP calculations will be discussed with the aid of symmetry decomposition and the investigation on the B_1 symmetry polarization.

In Fig. 3 we show our momentum-transfer cross section (MTCS), in the SE and SEP approximations, and that one of Kaur *et al.* [20] in the SEP approximation. There is an agreement in magnitude between the present SE results and the SEP momentum-transfer cross section obtained by Kaur *et al.* [20] but, our SEP calculations are below their results in the same approximation. Since the momentum-transfer cross section is obtained from the integration of the differential cross section with the $(1-\cos\theta)$ weighting factor, where θ is the scattering angle, the difference in magnitude of both MTCSs at low energy should not be related to how the long-range interaction is included, but to the other aspects of the calculations, such as the cc-pVTZ single-particle basis set (with one f type function on each heavy atom) used in the *R*-matrix calculations. The closest positions of our SE results with *R*-matrix method cross section in the SEP approximation could be due to a lack of polarization effects. Besides affecting the resonance's position, this may also affect the magnitude of their results.

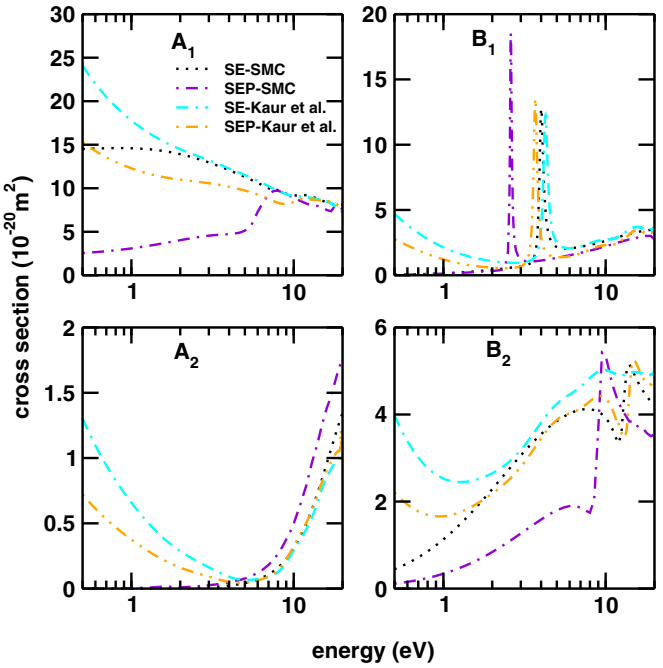

FIG. 4. Symmetry decomposition, in the C_{2v} point group, of the integral elastic cross sections for electron collisions with F_2CO molecules in the SE (dotted line) and SEP (dot-dashed line) approximations. TCS symmetry decomposition obtained by Kaur *et al.* [20] in the SE (dot-dash-dashed line) and SEP (dot-dot-dashed) approximations, both with the Born correction, is also shown. See text for discussion.

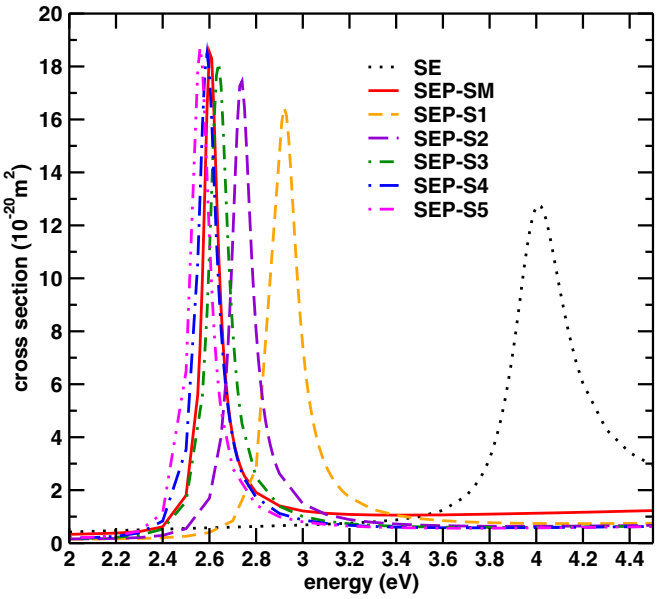

FIG. 5. B_1 symmetry cross section in the SE (dotted line) approximation, and in different increasing levels of polarization labeled SEP-S1 (short-dashed line), SEP-S2 (long-dashed line), SEP-S3 (dot-short-dashed line), SEP-S4 (dot-long-dashed line), and SEP-S5 (dot-dot-dashed line). The single MVO cross section, labeled SEP-SM (solid line), is also shown. The π^* resonance is centered at 4 eV (SE), 2.6 eV (SM), 2.9 eV (S1), 2.7 eV (S2), 2.64 eV (S3), 2.58 (S4), and 2.56 eV (S5). See text for discussion.

In Fig. 4 we show the symmetry decomposition of the integral elastic cross section in the SE and SEP approximations without the Born closure scheme. The A_1 symmetry shows, in the SE results, a monotonic decrease as energy increases, a shoulder at around 7 eV is present in the SEP calculations. The SEP results of Kaur *et al.* [20] for the A_1 symmetry show an increase in the cross section as energy vanishes; this symmetry is essentially the origin of the magnitude difference among the present integral and the total cross sections. The B_1 symmetry displays a π^* resonance at around 4.0 eV in the SE calculations that moves to around 2.6 eV with the inclusion of the polarization effects; here and in the integral cross section this symmetry was obtained from the SEP-SM calculation. The A_2 symmetry, in both SE and SEP results, shows an increase in the cross section with the increase of the incident electron energy. The B_2 symmetry has a shoulder centered at 14 eV in the SE calculations and the same shoulder is at around 10 eV in the SEP results. Despite having a resonantlike shape, the eigenphase analysis (not shown) of the A_1 and B_2 structures show that only the B_2 peak is a resonance. We have found a qualitative agreement with the results of Kaur *et al.* [20] but, for all the four symmetries, their SEP results are closer to the present SE calculations rather than to the SEP, and this fact also contributes to the proposition that their inclusion of polarization effects was not able to correctly describe the cross section in the low-energy range.

The cross sections for the B_1 symmetry in different levels of polarization are shown in Fig. 5. In the SE calculations the π^* state is located centered at 4 eV, and moves to around the folllowing: 2.92 eV in the S1 calculation, 2.73 eV in the S2 calculation, 2.63 eV in the S3 calculation, 2.59 eV in the S4 calculation, and 2.56 eV in the S5 calculation. This behavior suggests the polarization description is saturated, and the resonance is stable at 2.56–2.59 eV. The calculation using only the resonant MVO as scattering orbital puts the resonance at around 2.6 eV, corroborating the S1 to S5 results and with the experimental assignment at around 2.2–2.6 eV by Hoshino *et al.* [19]. The difference between the energy of the π^* state in the present SEP calculation and that of Kaur *et al.* [20] at the same level may be due to some lack of polarization in their calculations.

In order to explore the π^* character of the state located at 2.6 eV, we performed electronic structure calculations using the computational package GAMESS [39]. A minimal DZV basis set was employed in a Hartree-Fock calculation to obtain the plot contour of the b_1 LUMO, as shown in Fig. 6. The orbital related to resonance has the π^* character, being mainly located on the C=O bond and F atoms, in agreement with Kaur *et al.* and with the assignment proposed by Kato *et al.* [17] and by Hoshino *et al.* [19]. For low-lying π^* resonances, the vertical attachment energy VAE, which corresponds to the resonance position, can be obtained from the virtual orbital energy (VOE) by Koopmans' theorem through an empirical linear scaling relation [40]. We have applied an empirical scaling relation proposed by Aflatooni *et al.* [41] for the π^* resonance, where the geometry optimization and the VOE of the LUMO were obtained in the Hartree-Fock approximation with the 6-31G(d) atomic basis set. We obtained for the VAE the value of 1.5 eV, which is in qualitative agreement with the

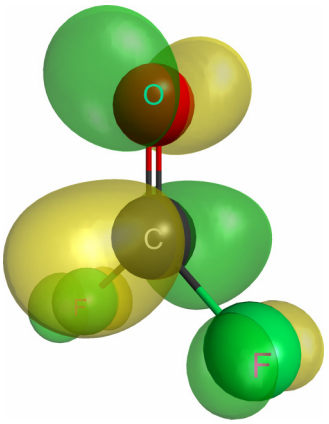

FIG. 6. Plot of the b_1 LUMO, mainly located out of the F–C=O plane, with a π^* character, and a major contribution around the C and O atoms, and a small one over the F atoms. The plot was generated with MacMolPlt [38]. See text for discussion.

present results. For the B_2 symmetry resonance, at 10 eV, the b_2 LUMO+2 (not shown) is an indication of this resonance; however, at this energy, a single unoccupied orbital being associated with the transient state is not a good model.

The differential cross sections for selected energies of the incident electron are shown in Fig. 7 in the SE and SEP approximations, both with and without the Born closure procedure. DCSs of Kaur *et al.* are also shown for comparison purposes. The Born closure scheme affects the magnitude of the DCSs for angles lower than 30° for 1 eV, 3 eV, and 6 eV, and for angles below 10° for 9 eV, 12 eV, and 15 eV. Analyzing the behavior of our SEP DCS, we can associate the major contribution of the following partial waves: p wave for 1 eV, 3 eV, and 6 eV, p and d waves for 9 eV, and d wave for 12 eV and 15 eV.

From the calculated DCS for the energies from 1 eV up to 9 eV, we note a great difference between SE and SEP approximations. This difference is due to the importance of a proper description of polarization effects at lower energies. Moreover, the fact that the calculated data of Kaur *et al.* agrees better at those energies with our SE than SEP DCSs corroborates our previous assertion of a poor description of the polarization effects by them. At higher energies, 12 eV and 15 eV, where the polarization effects are less pronounced, there is great agreement between our results at both SE and SEP approximations and the SEP data of Kaur *et al.* [20].

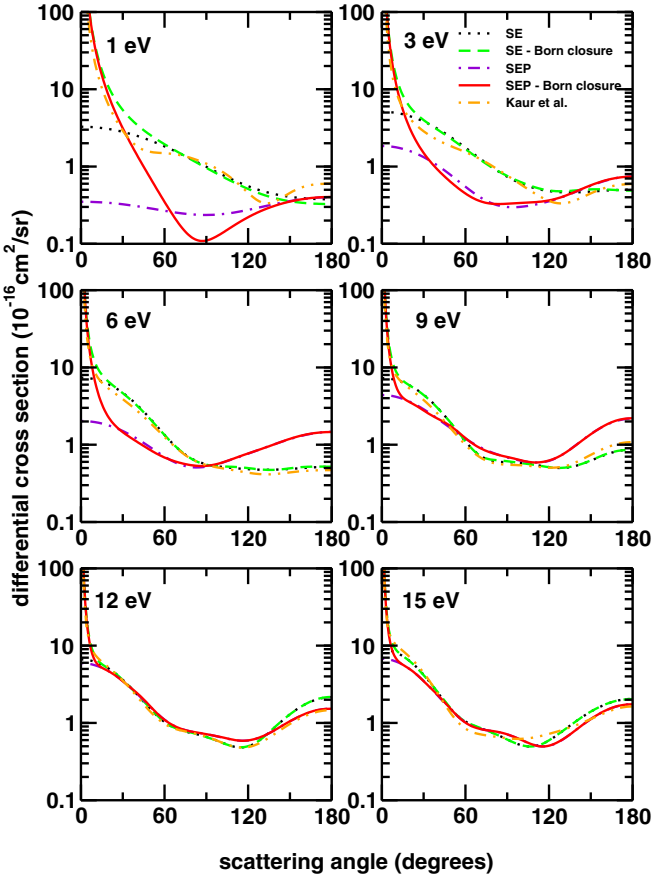

FIG. 7. Differential elastic cross sections for electron collisions with F_2CO molecules for selected energies of the incident electron in the SE (dotted line), SE with Born closure (dashed line), SEP (dot-dashed line), and SEP with Born closure (solid line) approximations. Calculated elastic DCSs by Kaur *et al.* [20] (dot-dot-dashed line), using the R-matrix method with polarization effects and Born correction, are also shown for comparison purposes. See text for discussion.

IV. CONCLUSIONS

In the present work we have calculated differential, integral, and momentum-transfer cross sections for elastic electron collisions with carbonyl fluoride, from the electron energy range of 0.5 eV to 20 eV. The low-lying π^* state was found to be centered at 2.6 eV after a systematic study to account for the polarization effects in the resonant B_1 symmetry. We also employed electronic structure calculations for a characterization of this shape resonance. We have found agreement with the available experimental data for the location in energy of the resonant state, but the results do not agree with the previous theoretical calculations, obtained with the R-matrix method. Another not previously reported B_2 resonance centered at 10 eV was also found. The differential cross section was compared with the ones available in the literature, with some qualitative agreement. The discrepancies found between the present calculations and the available theoretical data in the literature for the π^* state may be due to a less efficient polarization inclusion of the previous calculations.

ACKNOWLEDGMENTS

The authors acknowledge support from Brazilian agency CNPq. A.S.B. acknowledges support from Brazilian agency CAPES. M.H.F.B. also acknowledges support from FINEP (CT-Infra). The authors acknowledge computational support from Professor Carlos M. de Carvalho at DFis-UFPR and at LCPAD-UFPR. T.C.F. and M.F.H.B. also acknowledge computational support from CENAPAD-SP. The authors acknowledge J. Kaur and B. Antony for kindly providing their data in a tabulated form.

[1] See http://ozone.unep.org/en for the contents of the treatises about the ozone layer.
[2] J. Franklin, Chemosphere **27**, 1565 (1993).
[3] T. S. Dibble, M. M. Maricq, J. J. Szente, and J. S. Francisco, J. Phys. Chem. **99**, 17394 (1995).
[4] Y. Mitsui, Y. Ohira, T. Yonemura, T. Takaichi, A. Sekiya, and T. Beppu, J. Electrochem. Soc. **151**, G297 (2004).
[5] M. Riva, A. E. Lopez, D. Linaschke, I. Dani, and S. Kaskel, US Patent No. WO 2011032983 A2 (24 March 2011).
[6] J. Overend and J. R. Scherer, J. Chem. Phys. **32**, 1296 (1960).
[7] R. F. Miller and R. F. Curl, Jr., J. Chem. Phys. **34**, 1847 (1961).
[8] V. W. Laurie, D. T. Pence, and R. H. Jackson, J. Chem. Phys. **37**, 2995 (1962).
[9] V. W. Laurie and D. T. Pence, J. Mol. Spectrosc. **10**, 155 (1963).
[10] D. E. Milligan, M. E. Jacox, A. M. Bass, J. J. Comeford, and D. E. Mann, J. Chem. Phys. **42**, 3187 (1965).
[11] G. L. Workman and A. B. F. Duncan, J. Chem. Phys. **52**, 3204 (1970).
[12] M. B. Robin, *Higher Excited States of Polyatomic Molecules* (Academic Press, New York, 1975), Vol. 2.
[13] F. Grein, J. Phys. Chem. **102**, 10869 (1998).
[14] P. Sherwood, E. A. Seddon, M. F. Guest, M. J. Parkington, T. A. Ryan, and K. E. Seddon, J. Chem. Soc. Dalton Trans. **103**, 2359 (1995).
[15] E. Olalla, C. Lavín, A. M. Velasco, and I. Martín, Chem. Phys. Lett. **366**, 477 (2002).
[16] H. Choi and K. K. Baeck, Mol. Phys. **103**, 2247 (2005).
[17] H. Kato, C. Makochekanwa, M. Hoshino, M. Kimura, H. Cho, T. Kume, A. Yamamoto, and H. Tanaka, Chem. Phys. Lett. **425**, 1 (2006).
[18] H. Kato, Y. Nunes, D. Duflot, P. Limão-Vieira, and H. Tanaka, J. Phys. Chem. A **115**, 2708 (2011).
[19] M. Hoshino, P. Limão-Vieira, M. Probst, Y. Nunes, and H. Tanaka, Int. J. Mass Spectrom. **303**, 125 (2011).
[20] J. Kaur, N. Mason, and B. Antony, Phys. Rev. A **92**, 052702 (2015).
[21] K. Takatsuka and V. McKoy, Phys. Rev. A **24**, 2473 (1981).
[22] K. Takatsuka and V. McKoy, Phys. Rev. A **30**, 1734 (1984).
[23] M. A. P. Lima, L. M. Brescansin, A. J. R. da Silva, C. Winstead, and V. McKoy, Phys. Rev. A **41**, 327 (1990).
[24] M. H. F. Bettega, L. G. Ferreira, and M. A. P. Lima, Phys. Rev. A **47**, 1111 (1993).
[25] R. F. da Costa, M. T. do, N. Varella, M. H. F. Bettega, and M. A. P. Lima, Eur. Phys. J. D **69**, 159 (2015).
[26] NIST Computational Chemistry Comparison and Benchmark Database, NIST Standard Reference Database Number 101, 2016, edited by R. D. Johnson III, http://cccbdb.nist.gov/.
[27] G. B. Bachelet, D. R. Hamann, and M. Schlüter, Phys. Rev. B **26**, 4199 (1982).
[28] M. H. F. Bettega, A. P. P. Natalense, M. A. P. Lima, and L. G. Ferreira, Int. J. Quantum Chem. **60**, 821 (1996).
[29] F. Kossoski, M. H. F. Bettega, M. T. do, and N. Varella, J. Chem. Phys. **140**, 024317 (2014).
[30] G. M. Moreira and M. H. F. Bettega, Phys. Rev. A **93**, 062702 (2016).
[31] C. Bauschlicher, J. Chem. Phys. **72**, 880 (1980).
[32] B. I. Schneider and L. A. Collins, Phys. Rev. A **30**, 95 (1984).
[33] C. Winstead and V. McKoy, Phys. Rev. A **57**, 3589 (1998).
[34] S. H. D. M. Faria, J. V. da Silva, Jr., R. L. A. Haiduke, L. N. Vidal, P. A. M. Vazquez, and R. E. Bruns, J. Phys. Chem. A **111**, 7870 (2007).
[35] T. N. Rescigno and B. I. Schneider, Phys. Rev. A **45**, 2894 (1992).
[36] E. M. de Oliveira, R. F. da Costa, S. d'A. Sanchez, A. P. P. Natalense, M. H. F. Bettega, M. A. P. Lima, M. T. do, and N. Varella, Phys. Chem. Chem. Phys. **15**, 1682 (2013).
[37] M. T. do, N. Varella, M. H. F. Bettega, M. A. P. Lima, and L. G. Ferreira, J. Chem. Phys. **111**, 6396 (1999).
[38] B. M. Bode and M. S. Gordon, J. Mol. Graph. Model. **16**, 133 (1998).
[39] M. W. Schmidt, K. K. Baldridge, J. A. Boatz, S. T. Elbert, M. S. Gordon, J. H. Jensen, S. Koseki, N. Matsunaga, K. A. Nguyen, S. J. Su, T. L. Windus, M. Dupuis, and J. A. Montgomery, J. Comput. Chem. **14**, 1347 (1993).
[40] S. W. Staley and J. T. Strnad, J. Phys. Chem. **98**, 116 (1994).
[41] K. Aflatooni, G. A. Gallup, and P. D. Burrow, J. Chem. Phys. **132**, 094306 (2010).